Materials Transactions, Vol. 49, No. 10 (2008) pp. 2405 to 2413

EXPRESS REGULAR ARTICLE

The Effect of Microstructure Evolution on the Elevated Temperature Mechanical Properties in Mg-Sn-Ca System

Do Hyung Kim[1,*1], Ju Youn Lee[1,*1], Hyun Kyu Lim[1,*1], Joon Seok Kyeong[1,*1], Won Tae Kim[2] and Do Hyang Kim[1,*2]

[1]*Center for Noncrystalline Materials, Dept. of Metallurgical Eng., Yonsei University, 134 Shinchon-dong, Seodaemun-gu, Seoul 120-749, Korea*
[2]*Applied Science Division, Cheongju University, 36 Naedok-dong, Sangdang-gu, Cheongju, Chongbuk 360-764, Korea*

The effect of microstructural evolution on the creep properties in Mg-Sn-Ca system has been investigated. As-cast microstructure of Mg-Sn-Ca alloy consists of two or three phases depending on the Ca/Sn ratio, *i.e.* Mg_2Sn, CaMgSn and Mg_2Ca phases. Ternary CaMgSn phase has two types of morphology by its pseudo hyper-eutectic reaction with α-Mg; coarse rod-like primary or feather-like eutectic phase. Primary solidified CaMgSn phase exhibit negative effect on the tensile properties in spite of its high thermal stability up to 500°C. According to the creep test results, apparent stress exponent value ($n = 7$) indicates climb controlled creep mechanism by core diffusion above 150°C. Activation energy of Mg-5Sn-2Ca alloy (74 kJ/mol) is close to grain boundary diffusion for pure magnesium, 92 kJ/mol. Creep resistance is remarkably improved with the presence of Mg_2Ca phase. [doi:10.2320/matertrans.MER2008140]

(Received April 25, 2008; Accepted August 4, 2008; Published September 25, 2008)

Keywords: *magnesium-tin-calcium, creep, CaMgSn, Mg_2Ca*

1. Introduction

Mg alloys have the great potential for high performance structural applications due to their inherent properties such as low density, high specific strength, superior damping capacity and good castability etc. Commercial high temperature Mg alloys are often classified by their processing methods. There are Mg-Ag-RE, Mg-Zn-Zr and Mg-Y-RE series alloys which have been mainly fabricated by sand casting process. Though these alloys show high performance above 200°C,[1,2] their high cost by using rare earth elements restricts wider applications. Die cast processing is well known for high productivity. To improve die castability, most alloys contain Al. Although Al significantly increases castability, discontinuous precipitation of β-phase ($Mg_{17}Al_{12}$) significantly decreases high temperature strength.[3] Therefore, usage of Mg alloys containing Al is limited below 200°C.

Final goal for development of creep resistance Mg alloy is to design alloys with low cost, but maintaining its high performance. One of candidate for achieving this goal is Mg-Sn-Ca system. Basically, Sn and Ca have better cost effectiveness than rare earth elements. Moreover, according to the binary phase diagrams,[4] their inter-metallic compounds formed with Mg exhibit high thermal stability. Especially, there are a lot of successful developments on the enhancement of creep resistance in Mg-Al series alloy with Ca addition.[5–7]

In Mg-Sn binary system, Mg_2Sn phase has a high melting point (~770°C). In addition, this phase can be easily precipitated because it has a relatively high solubility limit (14.48 mass%) at 560°C and little solubility at ambient temperature. Lately, the alloys based on the binary Mg-Sn system have been received much attention for creep resistance alloy due to the high thermal stability of Mg_2Sn phase. Kang *et al.* reported that Mg_2Sn phase plays an important role in resisting matrix deformation during creep in Mg-8Sn-3Al-1Si alloy.[8,9] Kainer *et al.* have reported that ternary CaMgSn phase not only shows highly thermal stability up to 500°C, but also the alloys containing CaMgSn phase show favorable creep resistance in compressive mode.[10,11] More recently, A. Kozlov *et al.* have studied on the phase equilibria of Mg-Sn-Ca system using CALPHAD method.[12,13] However, close examination on the role of respective 2nd phases on high temperature mechanical properties has not been performed in detail. Therefore, in this study, the effect of microstructural evolution on the high temperature properties in Mg-Sn-Ca system has been investigated.

2. Experimental Procedure

All materials investigated in the present study are listed in Table 1. High purity metals with nominal compositions were prepared in an electrical resistance furnace under a $SF_6 + CO_2$ protective gas atmosphere. Molten metal was poured into a preheated (~100°C) rectangular steel mold with a dimension of 1.5 cm in thickness, 6 cm in width, and 10 cm in height.

The phases in as-cast microstructure of the alloys listed in Table 1 were analyzed preliminary via X-ray diffraction (Rigaku, CN2301) using monochromatic CuKα radiation to construct the phase selection map in as-cast state. For microstructural observations, the specimens were etched with a solution of 2% nital solution (2 ml nitric acid and 98 ml ethanol). The microstructures were observed by optical microscopy (OM; Leica DMRM) and scanning electron microscopy (SEM; JEOL 5310). A detailed analysis for phase identification was performed by transmission electron microscopy (TEM; JEM 2000 EX). Specimens for TEM were prepared by an ion milling method (Gatan, model 600) after mechanical grinding.

*[1]Graduate Student, Yonsei University
*[2]Corresponding author, E-mail: dohkim@yonsei.ac.kr

Uniaxial tensile tests were carried out on dog-bone specimens with constant cross head speed at an initial strain rate of $1 \times 10^{-3} \cdot s^{-1}$. Tensile creep tests were conducted by using direct loading type creep equipments. Cylindrical type creep specimens are precisely machined with a diameter of 6 mm and 25 mm gauge length.

Table 1 Chemical composition of all alloys prepared for this study.

No.	Composition (mass%)			Constitutive Phases	Abbrev.	Remarks
	Mg	Sn	Ca			
1	95	5	—	α-Mg, Mg_2Sn	T5	Mechanical properties
2	94	5	1	α-Mg, CaMgSn, Mg_2Sn	TX51	
3	93	5	2	α-Mg, CaMgSn, Mg_2Ca	TX52	
4	92	5	3	α-Mg, CaMgSn, Mg_2Ca	TX53	
5	91	5	4	α-Mg, CaMgSn, Mg_2Ca	TX54	
6	97.58	1.20	1.22	α-Mg, CaMgSn, Mg_2Ca	TX11	Phase construction map
7	88.15	11.10	0.75	α -Mg, CaMgSn, Mg_2Sn	TX111	
8	87.88	6.78	5.34	α-Mg, CaMgSn, Mg_2Ca	TX75	
9	93.23	1.18	5.59	α-Mg, Mg_2Ca	TX16	
10	98.70	0.48	0.82	α-Mg, CaMgSn, Mg_2Ca	TX01	
11	88.75	8.98	2.72	α-Mg, CaMgSn, Mg_2Sn	TX93	
12	85.33	10.97	3.70	α-Mg, CaMgSn	TX114	
13	92.70	6.91	0.39	α-Mg, CaMgSn, Mg_2Sn	TX70	
14	93.38	1.21	0.41	α-Mg, CaMgSn	TX10	

3. Results

3.1 As-cast microstructure analysis

Figure 1 describes as-cast state phase selection map for the alloys listed in Table 1. The alloy numbers corresponding to 14 alloys are also marked in the phase selection map. This map was constructed on the basis of phase identification results via X-ray diffraction method. As-cast microstructures of Mg-Sn-Ca alloy system consist of two or three phases depending on Ca/Sn ratio. From the X-ray diffraction result, constitutive phases were indentified as Mg_2Sn, CaMgSn and Mg_2Ca phases. The results of the phase identification are also listed Table 1. Two-phase regions of α-Mg + CaMgSn, α-Mg + Mg_2Sn, α-Mg + Mg_2Ca and three-phase regions of α-Mg + CaMgSn + Mg_2Sn and α-Mg + CaMgSn + Mg_2Ca are schematically outlined in Fig. 1 based on the result shown in Table 1. The Optical microscopic images shown in Fig. 1 stand for typical microstructures observed for the alloys listed in Table 1. As expected, T5 (Mg-5 mass%Sn) alloy consisted of two phase microstructure, α-Mg primary dendrite and interdendritic Mg_2Sn phases. With small addition of Ca, CaMgSn phase newly formed together with Mg_2Sn phase in TX51 (Mg-5 mass%Sn-1 mass%Ca) alloy. Noticeably, the ternary CaMgSn phase was present in two types of morphology; coarse rod-like phase in the grain interior and fine feather-like phase near inter-dendritic region. To identify these two types of the

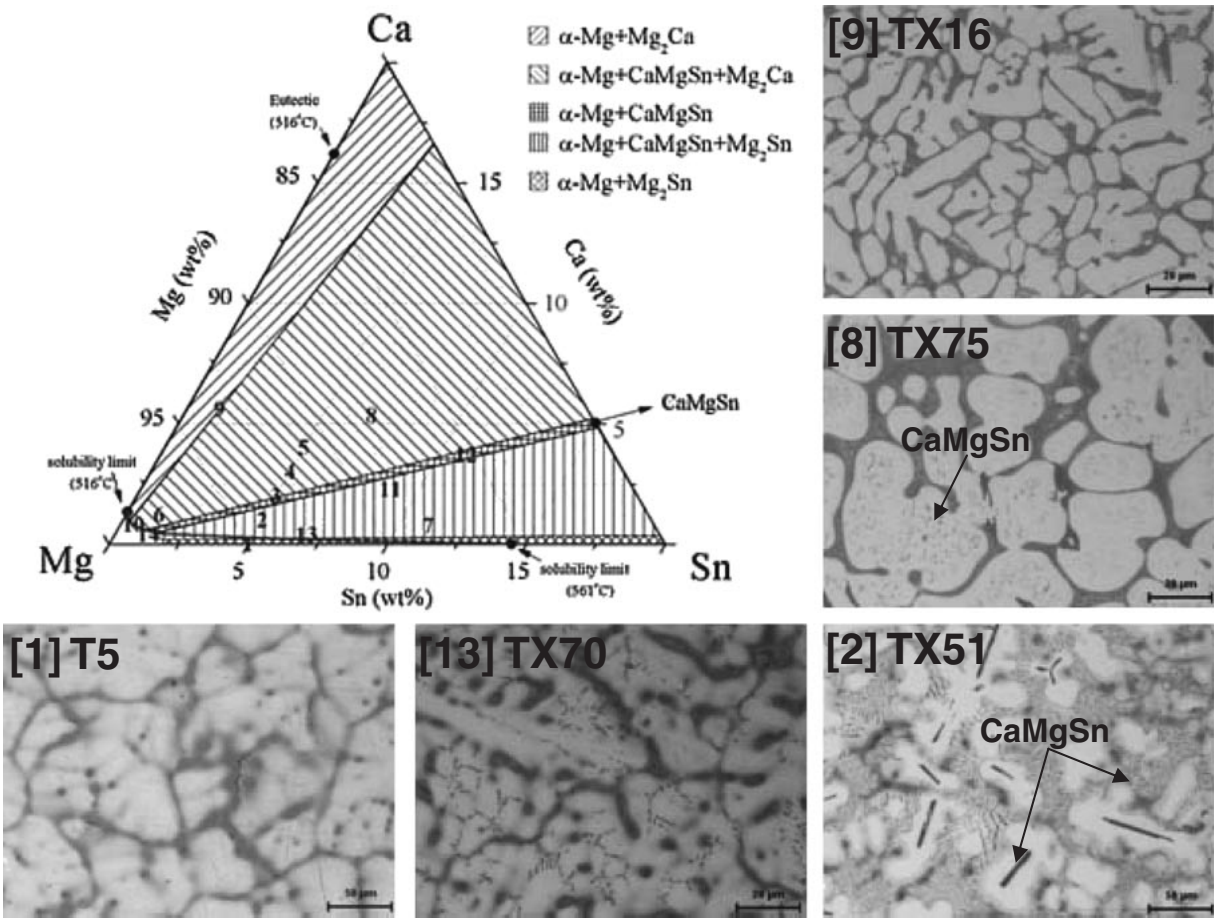

Fig. 1 Phase selection map for > 80 mass% Mg rich region obtained from as-cast state specimens.

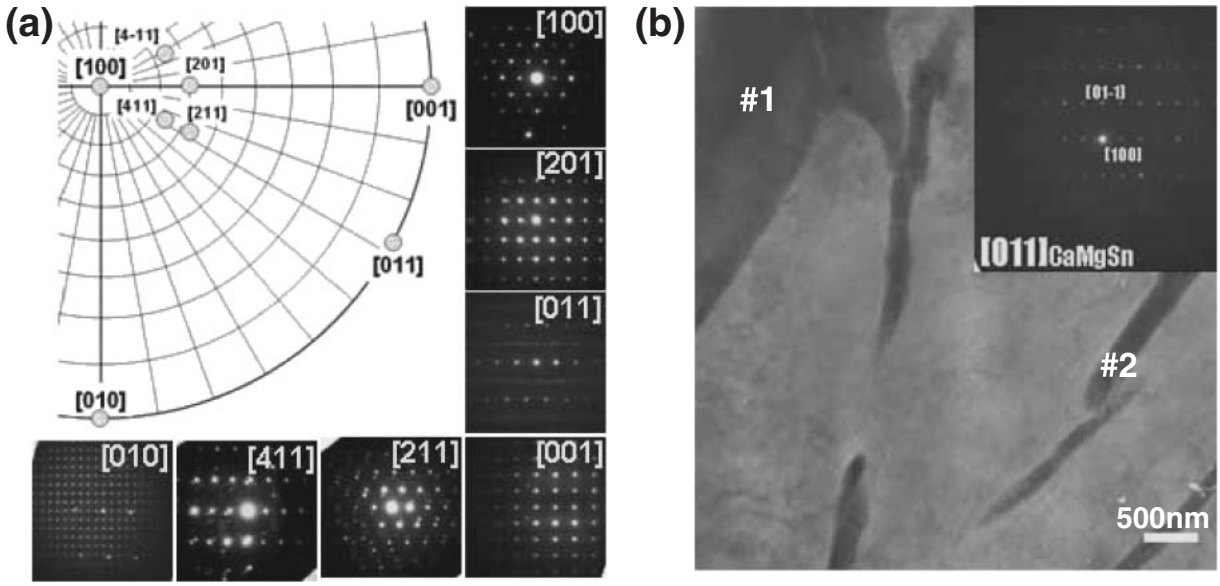

Fig. 2 Phase identification using transmission electron microscopy: (a) Stereogram at [100] zone axis of the CaMgSn phase constructed by several diffraction patterns obtained from feather-like phase; and (b) Selected area diffraction pattern obtained from coarse rod-like phase.

Table 2 EDS results obtained from CaMgSn phase as shown in Fig. 2(b).

EDS (at%)	Mg	Ca	Sn
#1	39.67	31.71	28.63
#2	38.97	27.09	33.94

phase carefully, TEM analysis was performed. Figure 2(a) is the stereogram centered at [100] zone axis constructed by several diffraction patterns obtained from feather-like phase, clearly confirming the primitive orthorhombic structure of CaMgSn phase. Besides, selected area diffraction pattern obtained from coarse rod-like phase corresponded to [011] zone axis of CaMgSn phase, as shown in Fig. 2(b). Energy dispersive spectrum (EDS) results obtained from coarse rod-like (#1 position in Fig. 2(b)) and fine feather-like (#2 position in Fig. 2(b)) phases are listed in Table 2, confirming that the composition of two-types of phase is nearly similar. TEM and EDS analysis support that two types of phase have same crystal structure in spite of the different morphologies. When the amount of Ca increased further or exceeds the amount of Sn, eutectic Mg_2Ca phase forms in inter-dendritic region as shown in TX16 (Mg-1 mass%Sn-6 mass%Ca) alloy. In the regions between three two-phase regions of α-Mg + CaMgSn, α-Mg + Mg_2Sn and α-Mg + Mg_2Ca, there are two three-phase regions of α-Mg + CaMgSn + Mg_2Sn and α-Mg + CaMgSn + Mg_2Ca as shown in TX70 (Mg-7 mass%Sn-0.5 mass%Ca) and TX75 (Mg-7 mass%Sn-5 mass%Ca) alloy, respectively.

Among the microstructures in Fig. 1, it is, in particular, noticeable that the ternary CaMgSn phase is present in two types of morphology when the alloy compositions are located in the two phase region of α-Mg and CaMgSn phases, coarse rod-like phase in the grain interior and fine feather-like phase near inter-dendritic region as shown in TX51 alloy. For detailed analysis on the solidification behavior, thermodynamic calculation was performed by using Pandat™ program. Figure 3(a) shows vertical-section between Mg and CaMgSn phase in ternary Mg-Sn-Ca system. There is a peudo-binary eutectic reaction between α-Mg and CaMgSn phase near the composition of 1 mass% Ca. Considering the optical microscope image of TX51 alloy in Fig. 1, the coarse rod-like CaMgSn phase forms as a primary solidification phase when passing through L + CaMgSn region in hyper-eutectic composition range during solidification. Primary CaMgSn phase grows with rod-like shape in the liquid melt at initial solidification stage. The optical microscope image of TX51 alloy in Fig. 1 also clearly shows that α-Mg halo forms around the primary CaMgSn phase. In general, when the composition difference between primary and the other eutectic phase is high enough, solute depleted zone easily forms around the primary solidification phase.[14] At the later stage of solidification, eutectic reaction occurs resulting in the formation of fine feather-like CaMgSn phase embedded in the α-Mg matrix since the pseudo-eutectic reaction composition is quite close to Mg. Figure 3(a) also shows that the pseudo-binary eutectic temperature is about 635°C. To confirm the thermal stability of the CaMgSn phase, TX51 alloy was annealed at 500°C for 24 h. For comparison, T5 alloy was annealed at the same condition. After heat treatment at 500°C, CaMgSn phase remained stable, but Mg_2Sn phase dissolved into the matrix in TX51 alloy (Fig. 3(c)), as can be seen clearly from the comparison with the as-cast microstructure of TX51 alloy in Fig. 1 (eutectic temperature of α-Mg and Mg_2Sn: 561°C). The result is further supported from the case of T5 alloy (Fig. 3(b)) where Mg_2Sn phase perfectly dissolves into the matrix. According to the thermodynamic data,[12] two invariant ternary eutectic reaction in Mg-rich region exist as follows; L $\rightarrow$ α-Mg + CaMgSn + Mg_2Sn at 561.81°C ($Mg_{88.92}Sn_{11.07}Ca_{0.01}$), L $\rightarrow$ α-Mg + CaMgSn + Mg_2Ca at 514.39°C ($Mg_{88.93}Sn_{0.20}Ca_{10.87}$). After pseudo-binary eutectic reaction, solidification is terminated by selecting one of two ternary eutectic reactions, depending on the alloy

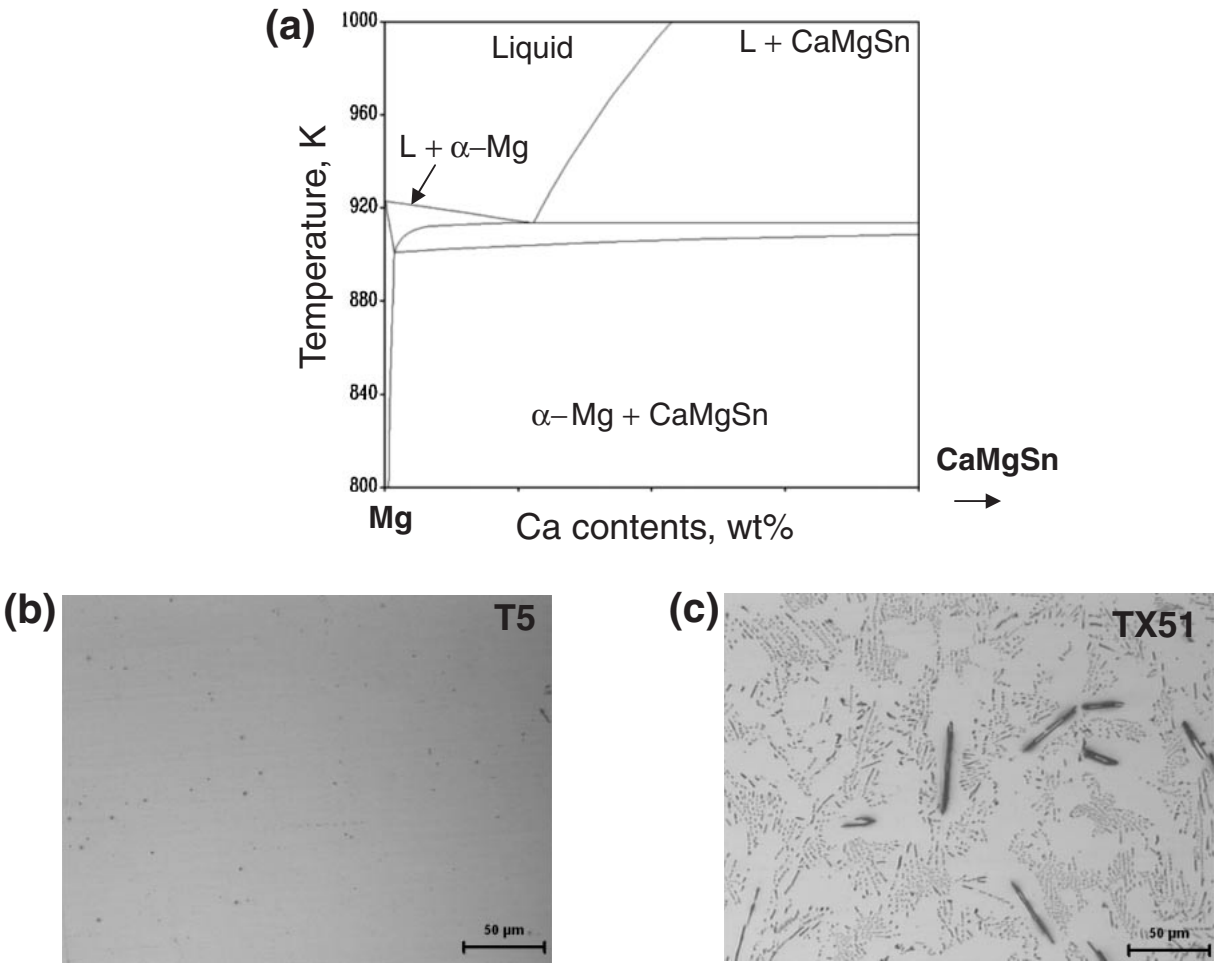

Fig. 3 (a) Cross-sectional phase diagram between α-Mg and CaMgSn phase constructed by thermodynamic calculation using Pandat™; and (b) Optical micrographs obtained from T5 and TX51 alloys after heat treatment at 500°C for 24 h.

composition. To predict the microstructure evolution more clearly, the solidification behavior was calculated by Scheil's model[15,16] (complete mixing in liquid, no diffusion in solid). The results about TX51 and TX52 alloy are described in Fig. 4(a) and (b). In both alloys, primary CaMgSn phase solidifies as a primary phase, and then pseudo binary eutectic reaction occurs at 638°C. However, final stage of solidification of remaining liquid in TX51 and TX52 is quiet different each other. In TX51 alloy, remained liquid solidifies by the ternary eutectic reaction; L $\rightarrow$ α-Mg + CaMgSn + Mg_2Sn at 561°C. On the other hand, in TX52 alloy, remained liquid solidifies by the ternary eutectic reaction; L $\rightarrow$ α-Mg + CaMgSn + Mg_2Ca at 514°C. Therefore, the phases which form at the final stage of solidification are Mg_2Sn and Mg_2Ca phases in TX51 and TX52 alloys, respectively. The solidification behavior of TX51 and TX52 alloys can be clearly evidenced from the as-cast microstructures shown in Fig. 4(a) and (b). The final solidified phases in ternary eutectic region were identified as Mg_2Sn and Mg_2Ca phase in TX51 and TX52 alloy, respectively, as marked by arrows in Fig. 4.

3.2 Mechanical properties at elevated temperature

Figure 5 describes the tensile test results of these alloys at room temperature and 200°C, respectively. T5 and TX51 alloys exhibited significant yield strength decrease at 200°C. Form the results of stress variations as shown in Fig. 5(c), it can be noticed that the high temperature yield strength remarkably improved above 2 mass% Ca. Compared with T5 alloy, the yield strength of TX51 alloy was also deteriorated significantly in spite of the existence of CaMgSn phase, indicating that primary and eutectic CaMgSn phase does not play a favorable role in enhancing the tensile properties. However, with increasing volume fraction of Mg_2Ca phase, high temperature strength was significantly improved, but ductility decreased (Fig. 5(b)).

Figure 6(a) shows the creep properties of T5 binary alloy. From the double logarithmic plot of stress as a function of minimum creep rate, stress exponent, n, is determined by following power law creep equation:[17]

$$\dot{\varepsilon} = A\sigma^n \exp\left(-\frac{Q}{RT}\right),$$

where $\dot{\varepsilon}$ is minimum creep rate (or secondary strain rate) and σ is applied stress, respectively. It can be observed that there is a significant variation in the stress exponent with stress and temperature. At the low stress regime, from the stress exponents ($n = 1$), it can be deduced that diffusional creep dominates the deformation behavior. At the medium stress regime, stress exponent of T5 alloy is increased from 3 to 7

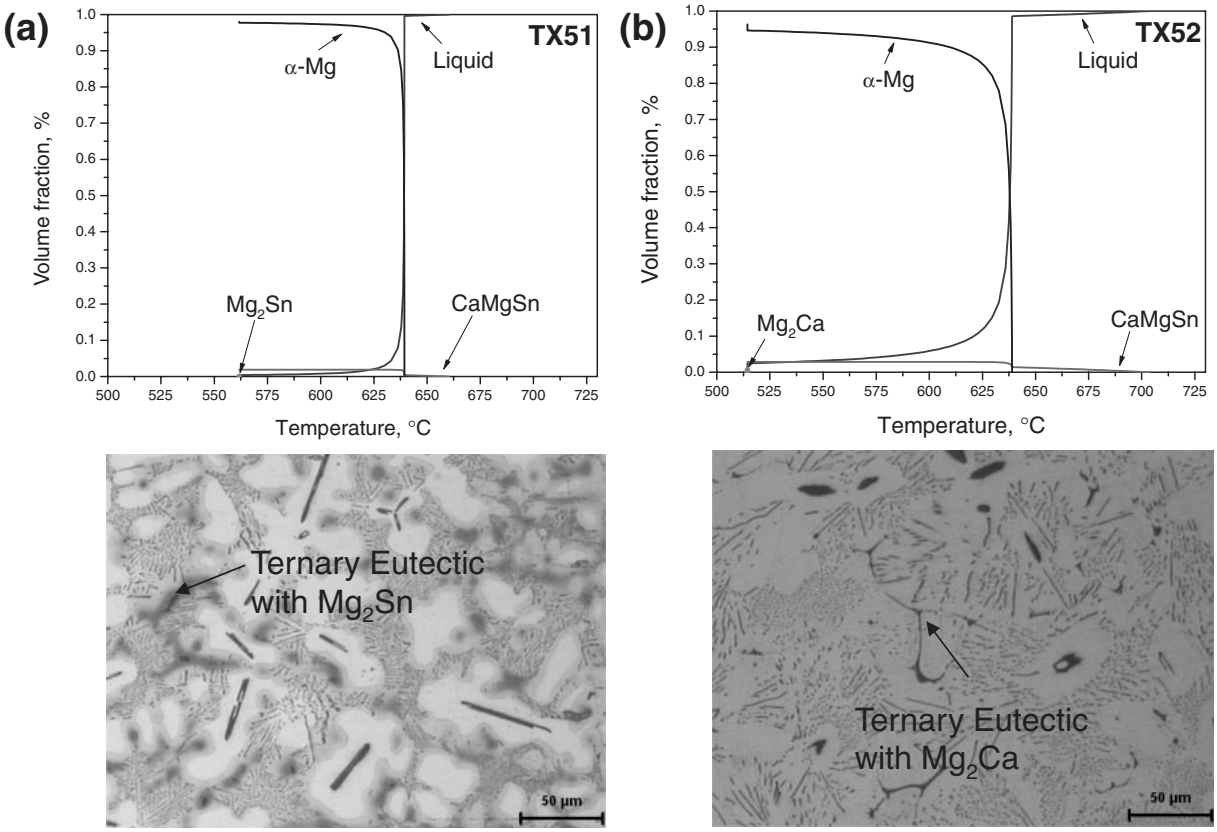

Fig. 4 Solidification behavior calculated using Scheil's model and comparison with optical microstructures in (a) TX51; and (b) TX52 alloy, respectively.

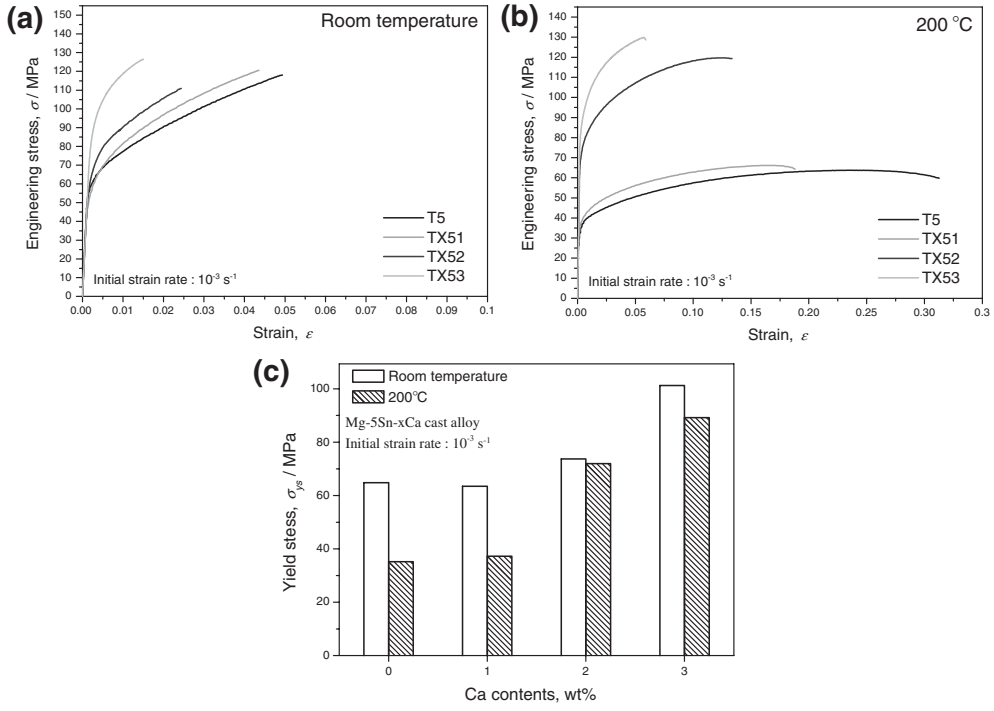

Fig. 5 Tensile test results of TX series alloys: (a) Stress-strain curves at room temperature; (b) Stress-strain curves at 200°C; and (c) Comparison of yield stress between room temperature and 200°C.

above 150°C. From these apparent stress exponents, creep mechanism changes from glide to climb controlled creep above 150°C. Detailed TEM analysis after creep deformation showed that dynamic precipitation of Mg_2Sn occurrs above 150°C as shown in Fig. 6(b). This precipitation may induce the increment of stress exponent. However, the effect of precipitation on the deformation behavior is not dealt with in detail in the present study.

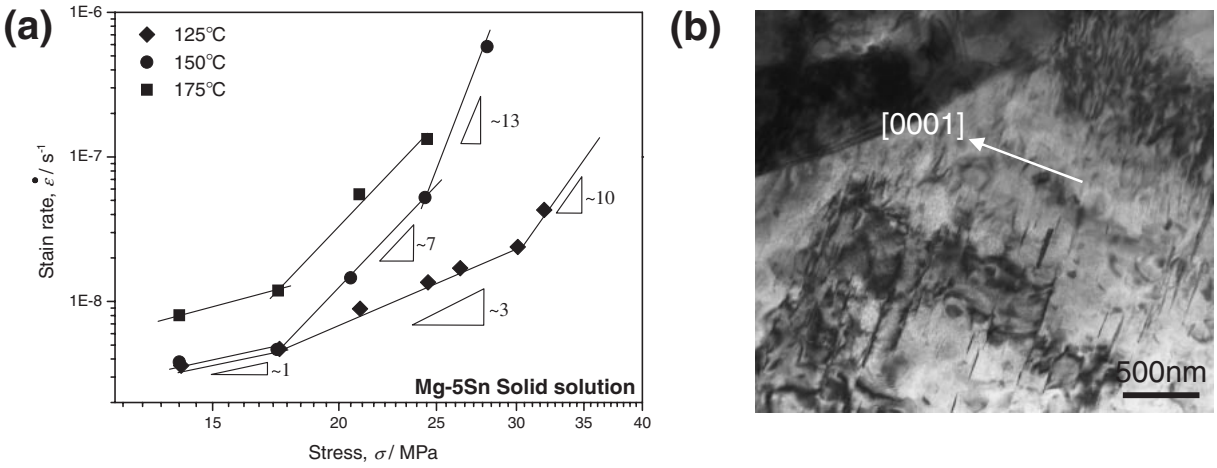

Fig. 6 Creep properties of T5 alloy: (a) Double logarithmic plot of stress as a function of minimum creep rate by power-law equation; and (b) Dynamic precipitation behavior in matrix after creep deformation at 150°C under 40 MPa.

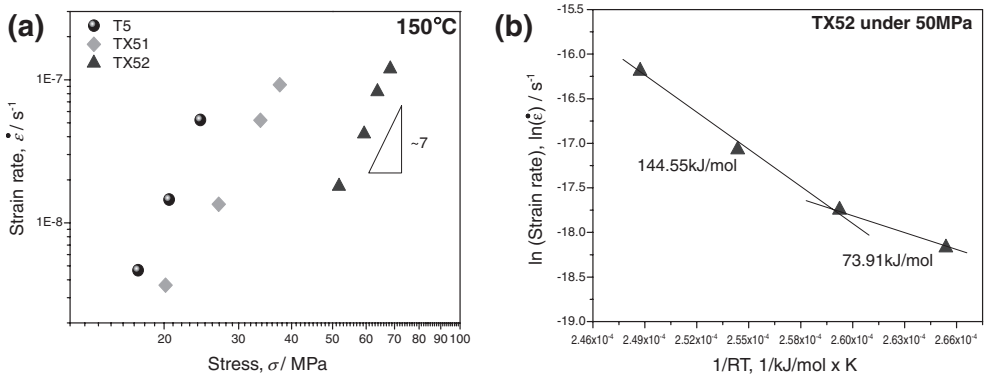

Fig. 7 Creep properties of TX series alloys: (a) Stress dependence behavior at 150°C; and (b) Temperature dependence behavior under 50 MPa in TX52 alloy.

Figure 7(a) shows creep properties of T5, TX51 and TX52 alloys at 150°C. Generally, when the Ca content increased, minimum creep rate decreased. Especially, creep resistance is remarkably improved above 2 mass% Ca content. This behavior shows similar tendency with the tensile test results at high temperature regime. Stress exponents of all the alloys show dislocation creep climb controlled behavior similar to T5 alloy. Figure 7(b) shows temperature dependence of creep behavior for TX52 alloy under 50 MPa. The activation energy of TX52 alloy was found to be 74 kJ/mol under loading condition of 50 MPa. This value is close to that of grain boundary diffusion for pure magnesium, 92 kJ/mol.[18] From the above results, high temperature mechanical properties are remarkably improved when the Ca contents increases above 2 mass%. According to the pre-described microstructure/phase analysis, this improvement attributed to the presence of Mg_2Ca phase.

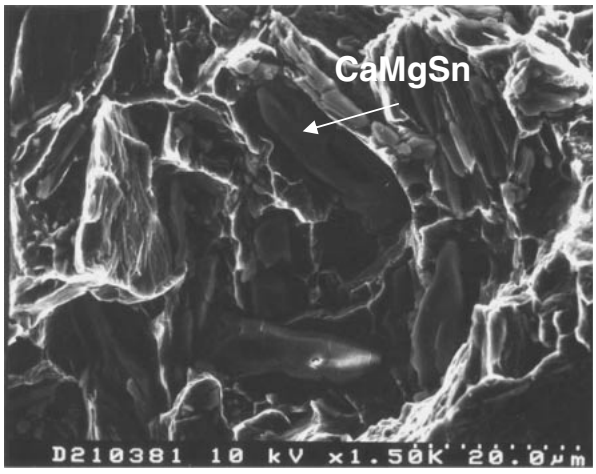

Fig. 8 Scanning electron microscope image obtained from fractured surface in TX51 alloy.

4. Discussion

4.1 The effect of morphology of CaMgSn phase on the mechanical properties

As mentioned above, CaMgSn phase has two types of morphology due to its pseudo eutectic solidification behavior. Though the CaMgSn phase shows high thermal stability, it does not provide beneficial effects on the tensile mechanical properties. This fact can be attributed to its solidification morphology of the CaMgSn primary phase. Figure 8 shows the fractured surface scanning electron microscopy (SEM) image after tensile test of TX51 alloy. It can be observed that primary CaMgSn phase acts as crack initiation sites during

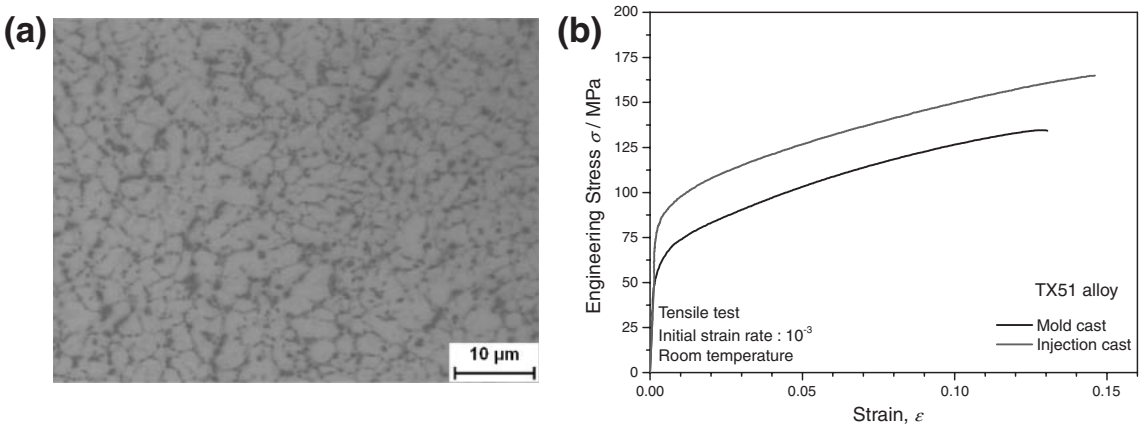

Fig. 9 Effect of cooling rate on tensile properties: (a) Optical microstructure of rapid solidified TX51 alloy; and (b) Comparison of tensile properties depending on the processing conditions.

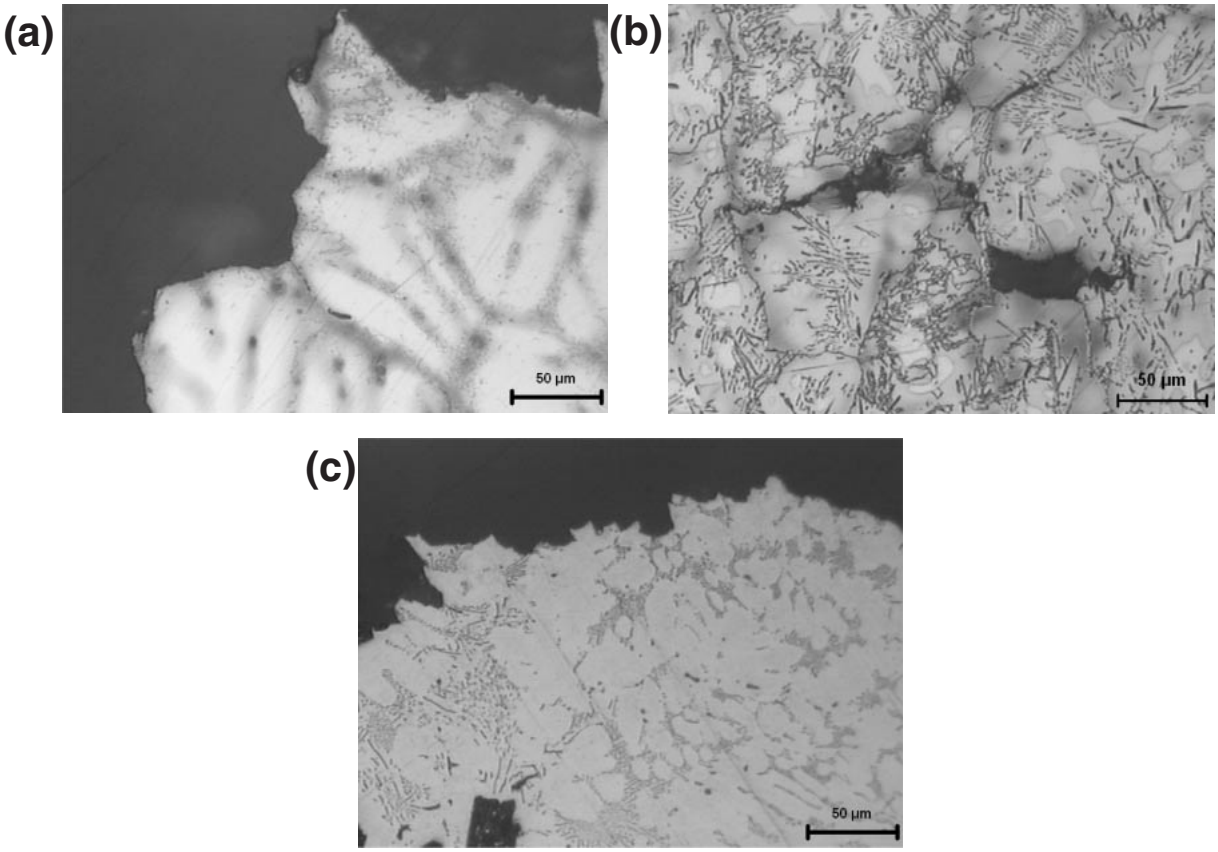

Fig. 10 Optical micrograph obtained after creep deformation at 200°C: (a) T5; (b) TX51; and (c) TX52 alloy, respectively.

deformation. Namely, ductile fracture is originated from the primary CaMgSn phase in grain interior. This means that primary CaMgSn phase can affect negatively on the tensile properties. In order to examine the effect of cooling rate on morphology of CaMgSn phase, rapidly solidified specimen by injection casting was prepared for mechanical test. In injection casting method, inductively re-melted sample in a fused silica tube is injected through a nozzle into water-cooled copper mold, having cylindrical cavity having 5 mm diameter and 50 mm height. Rapid cooling rate can effectively suppress growth of primary CaMgSn phase in TX51 alloy as shown in Fig. 9(a). According to the stress-strain curves obtained from tensile test, injection cast alloy shows higher mechanical properties than mold cast alloy (Fig. 9(b)). This result shows that formation of coarse primary CaMgSn phase can be avoided by high cooling rate processing. Further works about rapid cooling rate effect on the mechanical properties are in progress.

4.2 The effect of constituent phases on the elevated temperature properties

Figure 10 shows creep rupture behavior after deformation at 200°C. In the alloys containing Mg_2Sn phase, creep rupture occurs along the inter-granular boundary as shown in

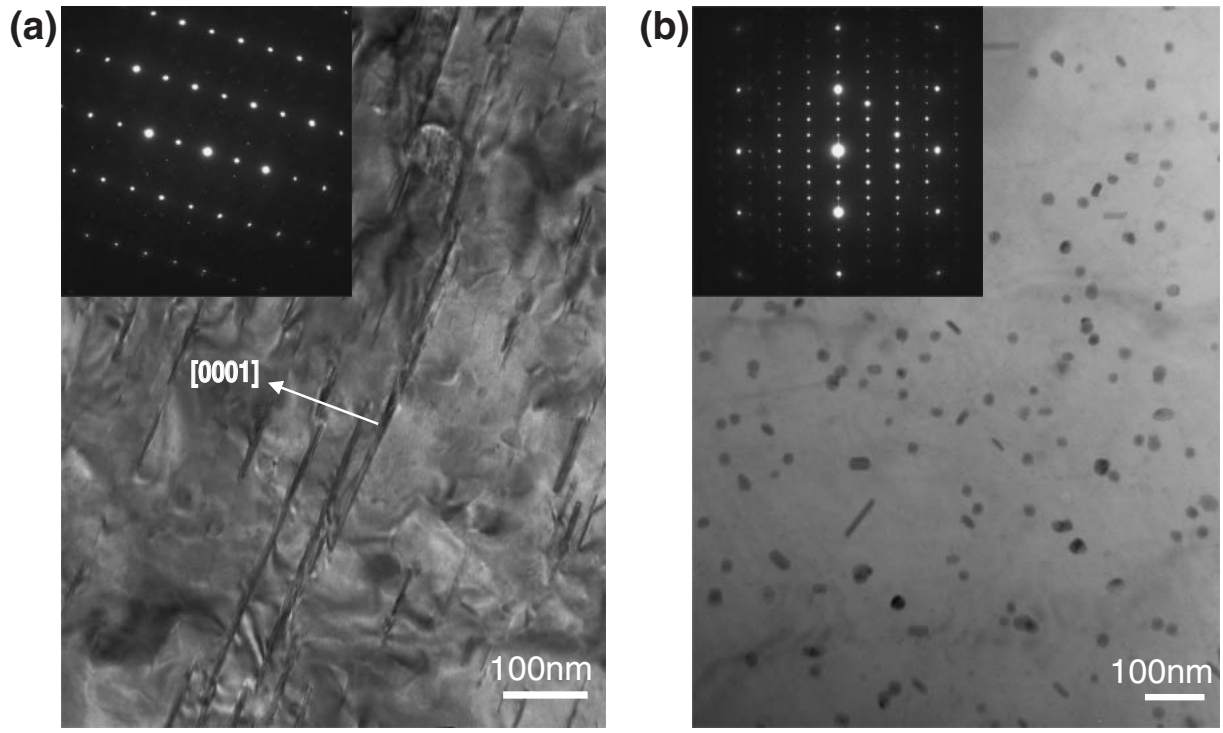

Fig. 11 Bight field images obtained from as-crept at 200°C: (a) T5 under 40 MPa loading. (b) TX53 alloy under 50 MPa loading, respectively.

Fig. 10(a) and (b). On the other hand, TX52 alloy containing Mg_2Ca phase shows trans-granular fracture as shown in Fig. 10(c). This means that eutectic Mg_2Ca phase shows better boundary strengthening than Mg_2Sn phase. Therefore, it is considered that Mg_2Ca phase effectively inhibits grain boundary sliding during creep deformation.

Figure 11 shows precipitation behavior of T5 and TX53 alloy after creep deformation at 200°C under 40 MPa and 50 MPa loading, respectively. As mentioned above, T5 alloy shows dynamic precipitation behavior. Mostly, rod-like Mg_2Sn precipitates lie along basal plane of α-Mg. Compared to the dynamic precipitation at 150°C as shown in Fig. 6(b), theses precipitates appears to be coarser. (Fig. 11(a)). On the other hand, in TX53 alloy, there is precipitation behavior, too. However, it can be observed that these fine precipitates remain stable without coarsening after creep deformation at 200°C. According to the selected area diffraction pattern, theses precipitates were identified as Mg_2Ca phase as shown in Fig. 11(b). Mg_2Ca precipitates exhibit various types of morphology; rod, spherical and short rod type. Rod-like precipitates have an orientation relationship with matrix; $(0001)_{Mg_2Ca} // (0001)_{Mg}$ and $\langle 2\bar{1}\bar{1}0\rangle_{Mg_2Ca} // \langle 10\bar{1}0\rangle_{Mg}$. This relationship corresponds to that reported in the previous report.[19] From these results, it can be deduced that Mg_2Ca precipitates are more effective on creep resistance than Mg_2Sn due to high thermal stability against coarsening.

5. Conclusions

In the present study, we have investigated the relationship between microstructural evolution and mechanical properties in Mg-Sn-Ca alloys. Major conclusions can be summarized as follows.

(1) As-cast microstructures of Mg-Sn-Ca alloy consist of two or three phase depending on the Ca/Sn ratio, *i.e.* Mg_2Sn, CaMgSn and Mg_2Ca phases.
(2) CaMgSn phase has two types of morphology due to its pseudo hyper-eutectic reaction with α-Mg, *i.e.* coarse rod-like primary phase and feather-like eutectic phase.
(3) Primary solidified CaMgSn phase exhibits negative effect on the tensile properties due to its solidification morphology.
(4) According to the creep test results of TX series alloys, apparent stress exponent value shows dislocation climb controlled mechanism by core diffusion ($n = 7$) above 150°C. Activation energy of TX52 alloy (74 kJ/mol) is close to grain boundary diffusion for pure magnesium, 92 kJ/mol.
(5) Creep resistance remarkably improves with the presence of Mg_2Ca phase. The Mg_2Ca phase changed the fracture behavior from inter-granular to trans-granular fracture mode. Mg_2Ca precipitates show higher thermal stability against coarsening that Mg_2Sn precipitates.

Acknowledgements

This study was supported by a grant from the Fundamental R&D Program for Core Technology of Materials funded by the Ministry of Commerce, Industry and Energy, Republic of Korea, and the Global Research Laboratory Program of Korea Ministry of Science and Technology. Ju Youn Lee, Joon Seok Kyeong and Hyun Kyu Lim are grateful for the support by Second Stage of Brain Korea 21 Program.

REFERENCES

1) B. L. Mordike: Mater. Sci. Eng. A **324** (2002) 103–112.
2) K. U. Kainer and F. von Buch: *Magnesium alloys and technology*, ed.

by K. U. Kainer, (Wiley-VCH, 2003).
3) C. J. Bettles and M. A. Gibson: *Magnesium Alloys and Their Applications*, ed. by K. U. Kainer, (Weinheim, 2004).
4) A. A. Nayeb-Hashemi and J. B. Clark: *Phase diagrams of binary magnesium alloy*, (ASM International, 1988).
5) Y. Terada, Y. Mori and T. Sato: Mater. Trans. **48** (2007) 97–100.
6) Y. Nakaura, A. Watanabe and K. Ohori: Mater. Trans. **47** (2006) 1031–1039.
7) Y. Terada, N. Ishimatsu, Y. Mori and T. Sato: Mater. Trans. **46** (2005) 145–147.
8) D. H. Kang, S. S. Park and Nack J. Kim: Mater. Sci. Eng. A **413–414** (2005) 555–560.
9) D. H. Kang, S. S. Park, Yoon S. Oh and Nack J. Kim: Mater. Sci. Eng. A **449–451** (2007) 318–321.
10) N. Hort, Y. Huang, T. A. Leil, P. Maier and K. U. Kainer: Adv. Eng. Mater. **8** (2006) 359–364.
11) T. A. Leil, Y. Huang, H. Dieringa, N. Hort, K. U. Kainer, J. Bursik, Y. Jiraskova and K. P. Rao: Mater. Sci. Forum **546–549** (2007) 69–72.
12) A. Kozlov, M. Ohno, R. Arroyave, Z. K. Liu and R. Schmid-Fetzer: Intermetallics **16** (2008) 299–315.
13) A. Kozlov, M. Ohno, R. Arroyave, Z. K. Liu and R. Schmid-Fetzer: Intermetallics **16** (2008) 316–321.
14) P. Gordon: *Principles of phase diagrams in materials systems*, (McGraw-Hill, 1968).
15) E. Scheil: Z. Metallkde **34** (1942) 70.
16) D. Stefanescu: *Science and Engineering of Casting Solidification*, (Kluwer Academic/Plenum Publishers, 2002).
17) T. H. Courtney: *Mechanical behavior of Materials*, (McGraw Hill Int. Ed. 2000).
18) H. J. Frost and M. F. Ashby: *Deformation-mechanism maps*, (Pergamon press, 1982).
19) J. F. Nie and B. C. Muddle: Scr. Mater. **37** (1997) 1475.